*Journal of Imaging Science and Technology*® 61(4): 040403-1–040403-10, 2017.


# Data Hiding by White Modulation in Color Direct Binary Search Halftones

**Vlado Kitanovski▲, Reiner Eschbach▲, Marius Pedersen▲, and Jon Yngve Hardeberg▲**
*The Norwegian Colour and Visual Computing Laboratory, Norwegian University of Science and Technology*
*E-mail: vlado.kitanovski@ntnu.no*

**Abstract.** *In this article, the authors propose a method for hiding a visual watermark in color printed images with arbitrary, natural content. The embedded watermark is imperceptible under normal illumination, but it is revealed under UV illumination. Their method is using the white-paper fluorescence as a source of the watermark signal. The binary visual watermark is embedded by controlling the amount of fluorescence during the halftoning process, which is achieved by modulating the fractional white area of exposed paper substrate. The method is based on the iterative Color Direct Binary Search halftoning, which ensures high quality of the printed images, and uses a suitable error metric to control the perceived distortion due to the watermark embedding. Results show that the proposed method achieves low perceptibility of the embedded watermark under normal illumination, while the watermark is easily detectable using a portable UV flashlight even in bright daylight conditions.*

[DOI: 10.2352/J.ImagingSci.Technol.2017.61.4.040403]

## INTRODUCTION

Data hiding in images, also known as image watermarking,[1] has been an active research area for the past few decades. While digital media is in the focus nowadays, printed media are still being used, and will be used in near future. A large number of documents still use the printed format, like breeder documents or internationally exchanged documents such as passports, educational diplomas and other transactional papers. Other examples of paper media are posters, certificates and any paper of value like tickets or vouchers. For all these printed formats there is a need for security features which can be used as an additional layer for authentication, source/ownership control or tamper detection. Techniques for data hiding in prints has also been studied for the past two decades; a small portion of these studies, relevant to our work, is briefly reviewed later in this section. Given that color print reproduction is relatively newer and more complex than monochromatic print reproduction, there is still ongoing research work focused on data hiding in color prints.

As printers are normally binary devices that either deposit colorant or not at any given location, prior to printing the digital content is binarized using a technique called halftoning. Halftoning exploits increased spatial resolution of printed dots to compensate for the lost amplitude resolution due to the binarization[2] (depositing colorant/ink or not). If it is not accounted for, halftoning may cause severe distortion to the embedded watermark data. This is the reason why many of the techniques for data hiding in prints embed the data during the halftoning process. Our proposed technique employs watermark detection that is purely visual—performed by a human subject. The main characteristics of visual watermark detection include relatively fast detection and robust detection due to the independency of imaging devices, geometric synchronization and/or stricter illumination conditions.

We present a brief survey of techniques for joint halftoning and data hiding in color printed images, where embedded data is graphic content and it is detected by visual inspection. The conjugate error diffusion in color images[3] is using two halftone images to hide binary visual pattern. The first halftone is obtained using the normal error diffusion to each of the color channels. The pixels in the second halftone are enforced, depending on the binary watermark, either to be the same (replicated) as in the first halftone or to be conjugated. The detection is performed by overlaying the two synced halftone images; the hidden watermark pattern reveals itself because the halftone area with enforced pixel conjugacy appears darker than the area with pixel replication. A similar method was proposed by Guo et al.,[4] where the conjugacy in the watermark areas is forced by coupling the same colorant channels of two, not necessarily identical images. The watermark detection is also performed by overlaying the halftones. Oztan and Sharma proposed a data hiding technique[5,6] for clustered-dot color halftones based on continuous phase modulation.[7] The phase of the colorant CMYK screens are altered according to the bit from the visual watermark pattern. The detection is visual—by overlaying appropriate non-phase-modulated halftone screen onto each of the colorant screens. Another method proposed[8] is utilizing a single stochastic screen for all CMYK colorants with successive filling and dot-on-dot printing geometry to embed data by forcing conjugacy in the regions where data is embedded. The detection is combined—the printed image is scanned as RGB, converted to grayscale and the detection of the pattern is performed visually. All of the presented techniques embed visual data by utilizing "conjugacy" in two or more halftones—the embedded data is revealed from the local increase/decrease of lightness due to the forced conjugacy of neighboring pixels from the two or more

▲ IS&T Members.

Received Mar. 1, 2017; accepted for publication June 10, 2017; published online July 19, 2017. Associate Editor: Henry Y. T. Ngan.
1062-3701/2017/61(4)/040403/10/$25.00

halftones. These techniques require accurate registration of printed halftone dots, and the detection requires additional halftone printed on a transparent substrate so that the two halftones can be overlaid to reveal the watermark.

Another group of techniques is using a specific illuminant to reveal the hidden watermark in the color printed image, which is imperceptible under normal light. Bala et al. proposed a method for visual watermark embedding in color prints, which uses optimal selection of metameres and narrowband light sources.[9] The metameric pairs are highly differentiable under the narrowband illumination due to significant difference in reflectances for the considered narrow wavelength range. Their approach for creating and selecting suitable metameres is by varying the gray component removal strategy. Authors observed that the main difference in measured reflectance is around the same wavelengths for most of the metameric pairs. This suggested using two narrowband light sources for detection that are tuned on those wavelengths (narrowband red and green light sources). Eschbach et al. proposed a watermarking method that exploits the infrared-reflecting property of paper substrates and infrared-absorbing property of carbon black toners.[10] The amount of the black colorant is modulated with the binary visual watermark by locally varying the gray component removal strategy. The embedded watermark is revealed under infrared illumination, using an infrared CCD sensor. Bala et al. proposed an approach[11] that exploits the fluorescent properties of Optical Brightener Agents (OBA) commonly present in paper substrates, and the UV-blocking properties of CMYK inks. The watermarking is formulated as an optimization problem of finding CMYK metameric pairs under normal illumination, which are realized by different ink–paper coverage and produce visible contrast under UV illumination. Zhao and Wang proposed a method for embedding a binary UV watermark in natural color images.[12] Their method is using two different clustered-dot halftoning strategies: one for the background, which appears darker under UV due to the dot-off-dot distribution, and another halftoning strategy for the watermark, which appears brighter under UV due to the dot-on-dot distribution of printer dots (hence, higher fractional area of paper substrate). The two different CMY halftoning algorithms are characterized, with the CIELAB space used as a connection space to build a look-up table for on-the-fly switching between the two halftoning strategies according to the binary watermark.

The focus of this work is data hiding in natural color printed images for visual detection under UV illumination by exploiting the paper substrate fluorescence. Given that common process inks are mostly blocking the UV light, the main approach for watermark signal embedding in this work is by changing/modulating the white-paper area. When the print is exposed under UV illumination, regions with different fractional white-paper coverage create visual contrast due to substantial difference in the fluorescence from those regions. Thus, the UV-exposable watermark is embedded in the image by spatially varying these regions with low and high fluorescence. Modulating the fractional white-paper area in a to-be-printed halftone, in general, results in changes that might be perceptible when the printed image is viewed under normal illumination as well. In this work, we propose a method for UV watermark embedding which is based on the Color Direct Binary Search (CDBS) halftoning algorithm.[13] In our joint halftoning and watermarking approach, we minimize the perceived error between the original and the printed image (without accounting for the paper fluorescence), while enforcing the fractional paper area according to the spatial watermark pattern. Our proposed method is closely related to two of the previously described methods. What they all have in common is the utilization of the paper fluorescence as a signal source for the binary UV watermark, and the variation of the fractional white-paper area to embed the UV watermark. Our method differs from the one of Bala et al.[11] in that it can be used on natural images with arbitrary content and color, not just on one metameric pair (two colors). The difference regarding the method[12] of Zhao and Wang is that our method is using frequency-modulated type of halftones, a single halftoning and watermarking strategy for the whole image, and our method is suitable for using an error metric during the halftoning process for uniform distribution of the watermarking distortion. The next section describes the proposed method and is followed by evaluation results and concluding remarks.

## METHODOLOGY FOR DATA HIDING BY WHITE MODULATION

This section starts with briefly introducing the Color Direct Binary Search halftoning algorithm, which is the basis for the data hiding by white modulation approach proposed in this work. It is followed by the proposed modification, which we refer through the text as Color Direct Binary Search-White Modulation (CDBS-WM), for modulating the fractional white area in color prints for UV-based data hiding by exploiting the paper fluorescence. The last subsection describes our approach of incorporating the $2 \times 2$ dot-centering printer model[14] into the CDBS-WM.

### *CDBS Halftoning*

The CDBS halftoning algorithm is an iterative halftoning algorithm, which minimizes perceived error between the continuous image and the halftone image. The perceived original image and the perceived halftone are obtained by filtering with point-spread functions (PSF). The initial halftone for the iterations is normally a random noisy pattern as this leads to avoiding any periodical patterns in the final converged halftone. During a single iteration, every halftone pixel is potentially modified (toggled) and swapped with each of its neighbors. The effects of these trial changes (7 possible toggles + 8 possible swaps for a 3-colorant halftone and $3 \times 3$ neighborhood) are evaluated so that only the change (if any) which reduces the perceived error the most is accepted. The halftone pixels are examined in several iterations until any possible pixel change does not reduce the perceived error. We

observed that full convergence normally happens after 15–40 iterations; but a very high quality and almost converged CDBS halftone is typically obtained only after 10 iterations,[15] regardless of the image content.

The total perceived error $E$ that is minimized in the CDBS is defined as:

$$E = \sum_i w_i \int |\tilde{e}_i(\mathbf{x})|^2 \, d\mathbf{x} \tag{1}$$

$$\tilde{e}_i(\mathbf{x}) = \sum_{\mathbf{m}} e_i[\mathbf{m}] \cdot p_i(\mathbf{x} - X\mathbf{m}) \tag{2}$$

$$e_i[\mathbf{m}] = f_i[\mathbf{m}] - g_i[\mathbf{m}]. \tag{3}$$

In Eqs. (1)–(3), $i$ identifies the channel of the color space that is used for error minimization, $\mathbf{x}$ and $\mathbf{m}$ are column vectors denoting continuous and discrete 2D coordinates respectively, $f[\mathbf{m}]$ and $g[\mathbf{m}]$ are the original image and the halftone image respectively, $p_i(\mathbf{x})$ is a continuous PSF for the $i$th color channel, the product matrix $\mathbf{Xm}$ addresses all of the discrete samples of the error image $e_i[\mathbf{m}]$. The weights $w_i$ are used to control the contribution of each color channel $i$ toward the total amount of perceived error. According to Eq. (2), the spatially continuous error $\tilde{e}_i(\mathbf{x})$ is effectively the continuous convolution between the PSFs $p_i(\mathbf{x})$ and the spatially discrete errors $e_i[\mathbf{m}]$ represented on a continuous spatial grid.

It has been shown[16] that the error $E$ can be calculated without actually performing the filtering with PSFs :

$$E = \sum_i w_i \sum_{\mathbf{m}} e_i[\mathbf{m}] \cdot c_{pe,i}[\mathbf{m}]. \tag{4}$$

In Eq. (4), the matrix $c_{pe,i}[\mathbf{m}]$ is the error $e_i[\mathbf{m}]$ convolved with the discrete autocorrelation function $c_{pp,i}[\mathbf{m}]$ of the PSF $p_i(\mathbf{x})$. The $c_{pe,i}[\mathbf{m}]$ matrices are calculated in the initialization stage, and they are progressively updated after every accepted trial change.

The impact of a trial change in the halftone $g[\mathbf{m}]$ to the error $E$ is given by:

$$\Delta E_T[\mathbf{m}_t] = \sum_i w_i \, ( \, b_i^2[\mathbf{m}_t] \cdot c_{pp,i}[0] + 2 b_i[\mathbf{m}_t] \cdot c_{pe,i}[\mathbf{m}_t] \, ) \tag{5}$$

$$\Delta E_S[\mathbf{m}_t, \mathbf{m}_s] = \Delta E_T[\mathbf{m}_t] + \Delta E_T[\mathbf{m}_s] + 2 \sum_i w_i b_i[\mathbf{m}_s] \cdot b_i[\mathbf{m}_t] \cdot c_{pp,i}[\mathbf{m}_s - \mathbf{m}_t]. \tag{6}$$

In Eq. (5), the error change due to a toggle at a pixel with coordinates $\mathbf{m}_t$ is denoted as $\Delta E_T[\mathbf{m}_t]$. In Eq. (6), the error change due to a swap between pixels at $\mathbf{m}_t$ and $\mathbf{m}_s$ is denoted as $\Delta E_S[\mathbf{m}_t, \mathbf{m}_s]$. The coefficients $b_i[\mathbf{m}_t]$ are equal to the pixel change in the minimization color space caused by the trial change—they are pre-computed and stored in a look-up table for fast access during the iterations. If the error change ($\Delta E_T[\mathbf{m}_t]$ or $\Delta E_S[\mathbf{m}_t, \mathbf{m}_s]$) is negative, it means that the trial change is reducing the total error $E$, so it is a possible candidate to become an accepted change. If the error change is positive, it means that the trial change is increasing the total error $E$ that we want to minimize, so this trial change is rejected. After all considered toggles and swaps within the pixel neighborhood are examined using Eqs. (5) and (6), the trial change which results in steepest error reduction (most negative $\Delta E$) is accepted, and the $c_{pe,i}[\mathbf{m}]$ matrices are updated using the following equation:

$$c_{pe,i,\text{new}}[\mathbf{m}] = c_{pe,i}[\mathbf{m}] + b_i[\mathbf{m}_t] \cdot c_{pp,i}[\mathbf{m} - \mathbf{m}_t] + b_i[\mathbf{m}_s] \cdot c_{pp,i}[\mathbf{m} - \mathbf{m}_s]. \tag{7}$$

The right-most product term in Eq. (7) corresponds to the second pixel of a swap at location $\mathbf{m}_s$, so if the accepted change is a toggle then the term is omitted.

### *White Modulation in CDBS*

In this subsection we describe the introduced modification to CDBS in order to control the fractional area of exposed paper substrate, or simply, the number of white pixels in the CDBS halftone. We call this modification of the CDBS "white modulation" (CDBS-WM) as effectively we are able to modulate visual watermark data by changing the fractional white area during the CDBS-like iterations. We do this by adding a term to the expression for the error that is minimized in the CDBS:

$$E = \sum_i w_i \int |\tilde{e}_i(\mathbf{x})|^2 \, d\mathbf{x} + F_W[\mathbf{m}]. \tag{8}$$

In Eq. (8), $F_W[\mathbf{m}]$ is a watermark term that is related to the total number of white pixels in the halftone, $N_W$:

$$F_W[\mathbf{m}] = \alpha k W_M[\mathbf{m}] N_W. \tag{9}$$

The parameter $\alpha (\alpha > 0)$ effectively controls the watermark signal strength as explained later. The constant $k (k > 0)$ is just a normalization constant that may as well be part of $\alpha$; however, we are formally using $k$ in order to avoid very small values for $\alpha$ that are of practical interest. The function $W_M[\mathbf{m}]$ is the spatial watermark pattern; it can have any value between the two extremes: "−1" corresponds to brighter parts of the watermark (halftone area with more white pixels), and "1" corresponds to the darker parts of the watermark (halftone area with less white pixels). In this work, the watermark pattern used is binary ($W_M[\mathbf{m}] \in \{-1, 1\}$), which maximizes the achievable watermark signal strength for given values of $k$ and $\alpha$.

The change to the minimization term $E$ in CDBS-WM due to a toggle at location $\mathbf{m}_t$ is given by:

$$\Delta E_T[\mathbf{m}_t] = \sum_i w_i (b_i^2[\mathbf{m}_t] \cdot c_{pp,i}[0] + 2 b_i[\mathbf{m}_t] \cdot c_{pe,i}[\mathbf{m}_t]) + \alpha k W_M[\mathbf{m}_t] \Delta N_W. \tag{10}$$

The only difference between Eqs. (5) and (10) is the right-most term introduced by $F_W[\mathbf{m}]$ in Eq. (8). The change of the number of white pixels $\Delta N_W$ due to a toggle can be either "−1," "0" or "1." This, combined with the binary spatial watermark value $W_M[\mathbf{m}_t]$ (that can be "−1" or "1") can lead to five possible cases:

1. The toggle does not change the number of white pixels ($\Delta N_W = 0$): The watermark term in Eq. (10) is zero regardless of $W_M[\mathbf{m}_t]$, Eq. (10) reduces to Eq. (5) so the toggle error change evaluation is the same as in the normal CDBS;

The following two cases are for toggling a non-white halftone pixel to white:

2. The toggle increases the number of white pixels ($\Delta N_W = 1$) and the watermark at that pixel is $W_M[\mathbf{m}_t] = -1$ (brighter part): The watermark term in Eq. (10) evaluates to $-\alpha k$,$\Delta E_T[\mathbf{m}_t]$ is drawn toward $-\infty$, and the toggle is more likely to be accepted because the accepted change is the one that results in most negative error change (most negative $\Delta E_T[\mathbf{m}_t]$). As a consequence, the higher the value of $\alpha$ is, the higher the number of halftone pixels (that correspond to brighter watermark part) is for which trial toggling to white will result in most negative $\Delta E_T[\mathbf{m}_t]$ and the toggle-to-white change being accepted. This increase of the amount of white pixels when increasing $\alpha$, in the halftone areas that correspond to the brighter part of the watermark pattern, effectively increases the strength of the perceived watermark under UV;

3. The toggle increases the number of white pixels ($\Delta N_W = 1$) and the watermark at that pixel is $W_M[\mathbf{m}_t] = 1$ (darker part): The watermark term in Eq. (10) evaluates to $\alpha k$,$\Delta E_T[\mathbf{m}_t]$ is drawn toward $+\infty$, and the toggle is less likely to be accepted because the accepted change is the one that results in most negative $\Delta E_T[\mathbf{m}_t]$. As a consequence, the higher the value of $\alpha$ is, the lower the number of halftone pixels (that correspond to darker watermark part) is for which trial toggling to white will result in most negative $\Delta E_T[\mathbf{m}_t]$ and the toggle-to-white change being accepted. This effective decrease of the amount of white pixels when increasing $\alpha$, in the halftone areas that correspond to the darker part of the watermark pattern, effectively increases the strength of the perceived watermark under UV;

The next two cases are for toggling a white halftone pixel to non-white pixel:

4. The toggle decreases the number of white pixels ($\Delta N_W = -1$) and $W_M[\mathbf{m}_t] = -1$ (brighter part): The watermark term evaluates to $\alpha k$,$\Delta E_T[\mathbf{m}_t]$ is drawn toward $+\infty$, so this toggle is less likely to be accepted. As a consequence, the higher the value of $\alpha$ is, the lower the number of white halftone pixels (that correspond to brighter watermark part) is for which trial toggling from white will result in most negative $\Delta E_T[\mathbf{m}_t]$ and the toggle-to-non-white change being accepted. This effective increase of the amount of white pixels when increasing $\alpha$, in the halftone areas that correspond to the brighter part of the watermark pattern, effectively increases the strength of the perceived watermark under UV;

**Table I.** Impact of the watermark term on the error change due to a trial toggle at pixel position $\mathbf{m}_t$.

| | Pixel $\mathbf{m}_t$ belongs to the brighter part of the binary watermark $W_M[m]$ | Pixel $\mathbf{m}_t$ belongs to the darker part of the binary watermark $W_M[m]$ |
|---|---|---|
| The trial toggle at $\mathbf{m}_t$ is from non-white pixel to white pixel | $-\alpha k$ | $\alpha k$ |
| The trial toggle at $\mathbf{m}_t$ is from white pixel to non-white pixel | $\alpha k$ | $-\alpha k$ |

5. The toggle decreases the number of white pixels ($\Delta N_W = -1$) and $W_M[\mathbf{m}_t] = 1$ (darker part): The watermark term evaluates to $-\alpha k$,$\Delta E_T[\mathbf{m}_t]$ is drawn toward $-\infty$, so this toggle is more likely to be accepted. As a consequence, the higher the value of $\alpha$ is, the higher the number of white halftone pixels (that correspond to brighter watermark part) is for which trial toggling from white will result in most negative $\Delta E_T[\mathbf{m}_t]$ and the toggle-to-non-white change being accepted. This decrease of the amount of white pixels when increasing $\alpha$, in the halftone areas that correspond to the darker part of the watermark pattern, effectively increases the strength of the perceived watermark under UV.

In Table I, we summarize the impact of the watermark term in Eq. (10) to the trial toggle error change $\Delta E_T[\mathbf{m}_t]$ for the four cases (2–5) that involve white pixels and that are directly used for white modulation. In the two diagonal cells, it can be seen that the error change $\Delta E_T[\mathbf{m}_t]$ is drawn toward $-\infty$ for amount $\alpha k$ (making the trial toggle more likely to be accepted) when the trial toggle is effectively embedding the watermark—increasing the number of white pixels in the brighter watermark parts and decreasing the number of white pixels in the darker watermark parts.

In short, the value of the watermark product term $\alpha k$, defines the minimum amount of decrease in perceived error $E$ (as defined in Eq. (1), without the watermark term) due to the toggle, which is needed to outweigh the white pixel enforcement/denial from the introduced watermark term. As the perceived error is well correlated to the squared Euclidean distance (between the perceived original and halftone image) in the minimization color space, it is important to use a perceptually uniform color space for the error minimization—this will result in more uniform distribution of distortion for different parts of the printer gamut due to the white modulation.

In this work, initially we used the linearized CIELAB space denoted as $Y_yC_xC_z$ space[17] for perceived error minimization, as proposed in the normal CDBS. The used weights for the three channels were: $w_{Yy} = 1$, $w_{Cx} = w_{Cz} = 0.25$. Initial tests showed that the amount of perceptible distortion for a given value of $\alpha$ varies a lot for different parts of the printer gamut. In order to achieve higher uniformness, we

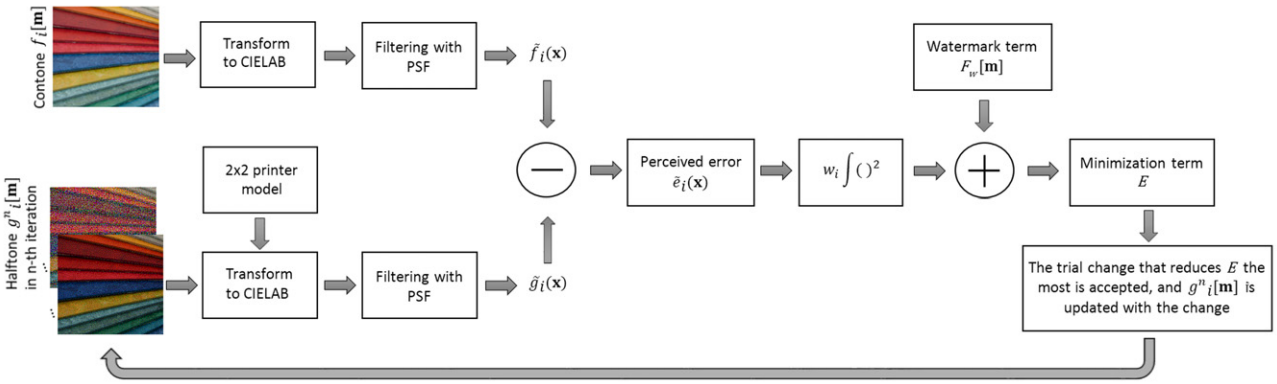


Figure 1. Simplified flow-chart of the CDBS-WM algorithm.

used the CIELAB space to express the perceived error during minimization. The trials showed that the visible distortion due to white modulation is noticeably more uniform for different hues and for different lightness values. In the rest of the work, we used the CIELAB space for CDBS-WM.

It needs to be noted that when it comes to halftone texture quality, the most important parameters for the CDBS-WM algorithm (and for the CDBS in general) are the weights $w_i$ and the PSFs $p_i(\mathbf{x})$ used for each of the color channels. The CIELAB space was not used as error minimization space in previous work due to its property of not preserving local averages[13,17] or due to resulting in more grainy halftone textures.[18] However, for watermarking in natural images, perceptual uniformness is also very important, so we decided to use the CIELAB space and try to obtain nearly optimal parameter settings for this color space. We tested various combinations of different weights $(w_{L^*} = 1, w_a, w_b)$ with different PSFs $(p_{L^*}(\mathbf{x}), p_a(\mathbf{x}), p_b(\mathbf{x}))$ of Nasanen type[19] that resulted in more homogeneous prints in previous works.[13,20] The combination that resulted in finest halftone texture and relatively strong watermark signal was: $w_{L^*} = 1$, $w_a = 0.35$, $w_b = 0.15$; $p_{L^*}(\mathbf{x})$ of Nasanen type for viewing distance of 12.7 cm (5 inches); $p_a(\mathbf{x})$ and $p_b(\mathbf{x})$ of Nasanen type for viewing distance of 17.8 cm (7 inches). The unusual short viewing distance for the PSFs means that their spatial support is relatively short, which reduces the effect of non-preserving averages and it leads to finer halftone textures. We used this parameter setting for all of the prints in this work.

The effect of a swap is not considered in this work, as swaps do not change the total number of white pixels; even when white pixels are involved in a swap, the watermark terms will cancel out for vast majority of the image pixels. The only case when swaps may be considered for white modulation is when the watermark pattern has different values for the two pixels involved in the swap, i.e., $W_M[\mathbf{m}_t] \neq W_M[\mathbf{m}_s]$. These cases may occur only for the pixels on the edges of the binary watermark pattern and they are relevant only if white pixels are involved in the swap. Due to the negligible number of such cases, and in order to avoid computational overhead, swaps are not considered for white modulation in this work. Thus, the evaluation of the impact of a trial swap on the error change stays the same as in the normal CDBS—by using Eq. (6).

The flow-chart of the iterative CDBS-WM method is given in Figure 1. Please note that this is an equivalent scheme, because no actual filtering with PSFs is needed after every accepted change in the halftone during the iterations.[13,15,16] The impact of the trial changes on the minimization term can be efficiently calculated using Eqs. (5)–(6). The impact of the watermark term is added to the former (using Eq. (10)) and the result is compared to all other trial changes for the given pixel. The change that decreases (if any) the minimization term the most is accepted.

### 2 × 2 *Dot-Centering Printer Model*

We use a printer model to estimate the printer output in a well-defined color space, so that we can further optimize the visibility of the watermark or the perceptibility of the introduced distortion. In this work, we used the 2 × 2 dot-centering printer model[14] that is also used in the original CDBS work.[13] The 2 × 2 centering model is a measurement-based model that accounts for ink dots overlapping in color halftones. It uses the notion of "rendered image" with the same dimension as the halftone but with both 2D pixel coordinates shifted for half pixel, as shown in Figure 2. In that way, every pixel of the rendered image is affected by four 2 × 2 halftone pixels, and every halftone pixel affects four 2 × 2 pixels in the rendered image. Thus, the model implicitly assumes that the dot overlap is limited to half of the dot area.

In order to characterize a printer using this method, all of the possible 2 × 2 colorant combinations are printed and measured by a spectrophotometer. If all possible colorant overprints are allowed, the total number of different patches to be measured for characterization is $(2^N)^4 = 16^N$, where $N$ is the number of inks. In order to incorporate the 2 × 2 model into our modified CDBS, we made the following steps:

1. We use only CMY colorants, so the total number of 2 × 2 patches is 4096. We assumed horizontal and vertical symmetry of the printer dots, which reduced the total number of patches to 1072. These 1072 patches

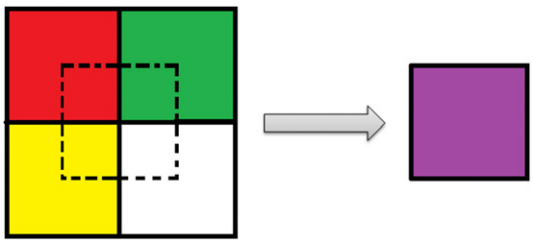

Figure 2. 2 × 2 dot-centering model: Four 2 × 2 halftone dots contribute to one pixel in the rendered image.

were printed, measured with a spectrophotometer, and the measured reflectances were converted to the CIELAB space, assuming standard D50 illuminant and 2° standard observer. It is important to note that the proposed technique is not restricted to CMY printing. However, using more inks will increase the number of measured 2 × 2 patches, and more importantly, will increase the size of the look-up table for the printer color space to CIELAB conversion. For example, if we use four CMYK colorants, the CMYK-to-CIELAB look-up table will be 256 times larger than the CMY-to-CIELAB look-up table. Therefore, this 2 × 2 printer model is impractical for characterizing multi-channel printers.

2. The CDBS perceived error (Eq. (1)) is defined for the 2 × 2 rendered image and it is expressed in the CIELAB space. This requires converting both the original sRGB image and the initial CMY halftone to CIELAB for the $c_{pe,i}[\mathbf{m}]$ initialization. Given that the sRGB gamut is larger than the CMY gamut, we shrink the CIELAB values of the original image by empirically chosen factor of 1.05. We chose a naïve gamut-compression approach to reduce saturated/clipped areas that, in general, are not very suitable for modulating white pixels. The gamut mapping between sRGB and CMY is an issue which can be addressed separately; however, it is not in the focus of this work;

3. The evaluation of a toggle effect is more complex because a single toggle in the halftone image directly influences the corresponding 2 × 2 pixels in the rendered image. If we denote these 2 × 2 pixels corresponding to halftone location $\mathbf{m}_t$ with $\Gamma_{\mathbf{m}_t}$, the error change in the rendered image due to a toggle at location $\mathbf{m}_t$ is given by:

$$\Delta E_T[\mathbf{m}_t] = \sum_i w_i \sum_{n\in\Gamma_{\mathbf{m}_t}} \sum_{k\in\Gamma_{\mathbf{m}_t}} b_i[n]\cdot b_i[k]\cdot c_{pp,i}[n-k] + \sum_i w_i \sum_{n\in\Gamma_{\mathbf{m}_t}} 2b_i[n]\cdot c_{pe,i}[n] + \alpha k W_M[\mathbf{m}_t]\Delta N_W. \quad (11)$$

The watermark term (the right-most term) in Eq. (11) is the same as in Eq. (10) because it is defined on the printer (halftone) grid; it is only the term for the CDBS perceived error that needs to include the effect of rendered image 2 × 2 pixels change;

4. The $b[\mathbf{m}]$ coefficients in Eq. (11) define the CIELAB shifts in the rendered image due to a toggle. They are drawn from a 4096 × 4096 look-up table, which is generated from the measurements in step 1;

5. If a change is accepted, then the $c_{pe,i}[\mathbf{m}]$ matrices are updated using:

$$c_{pe,i,\text{new}}[\mathbf{m}] = c_{pe,i}[\mathbf{m}] + \sum_{n\in\Gamma_{\mathbf{m}_t}} b_i[n]\cdot c_{pp,i}[\mathbf{m}-n] + \sum_{k\in\Gamma_{\mathbf{m}_s}} b_i[k]\cdot c_{pp,i}[\mathbf{m}-k]. \quad (12)$$

In Eq. (12), the second term on the right is the update due to a toggle; the right-most term is due to the second toggle of a swap.

## RESULTS AND EVALUATION

The CDBS-WM algorithm was implemented as single-threaded in C/C++, and it was initialized with the same randomized CMY halftone for all samples used in this work. The total execution time for a 1 megapixel image is around 34 seconds on the i7-5600U CPU. An MS Windows demo application for CDBS-WM is available for download at: http://www.colourlab.no/cid. The algorithm's execution time may be significantly reduced by using a block-based search strategy[21] and/or parallelizing the implementation.[22] We printed our CDBS-WM CMY halftones through the Caldera RIP software on 130 g/m$^2$ HP Heavyweight Coated paper using the HP DesignJet Z3200 printer. The printing resolution for all of test images was set to 300 dpi. We used the X-Rite i1 spectrophotometer for measuring the 2 × 2 calibration patches, also printed at 300dpi. Figure 3 (left) shows an example of a CDBS-WM printed image as seen in an office environment. The embedded binary pattern is shown on Fig. 3 (right). When a UV flashlight is held above the image, the result changes to the image in Fig. 3 (middle).

Note that in this example we added the UV light to the room illumination, rather than replacing the room illumination. Adding UV light to the room light reflects a more likely usage scenario and thus gives an indication of overall UV-signal strength. Since CDBS-WM is a pixel-wise operation, we also examined the printout under the microscope using different illuminations. This is shown in Figure 4 for a different image. Fig. 4 (left) shows an edge area with the print dots clearly visible. The identical area is then observed under UV illumination showing the letter "U" as part of the watermark. From Fig. 4 one can see that white modulation for watermarking is clearly influenced by the local image content. For example, in a white, or very bright, region, no watermark modulation will be easily seen since there is already a large number of white pixels (Fig. 4 lower-right part). In dark regions, only a small number of white pixels can be forced into the desired rendering. However, as can be seen from Fig. 3 the overall impression of the watermark stays intact. In order to see the trade-off between watermark visibility under UV illumination and

Figure 3. Printout as seen under room illumination (left) and the identical printout when a UV light is added (middle). The embedded CDBS-WM binary pattern is shown on the right.

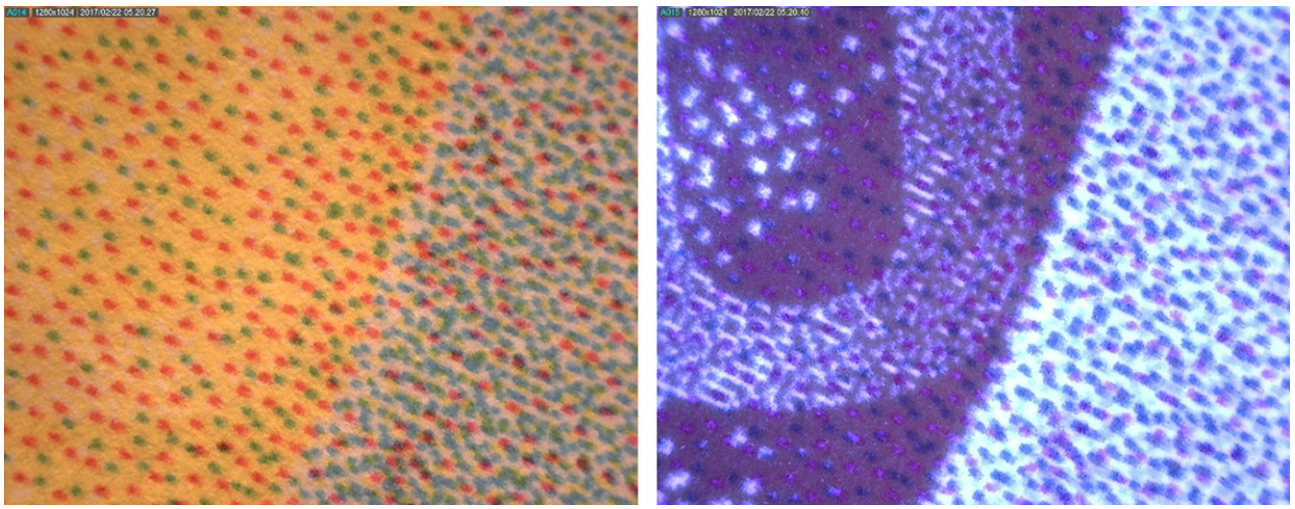

Figure 4. A different image viewed under the microscope. The image under daylight (left) shows the microstructure of an edge area and the UV illumination (right) shows the identical area. The letter "U" which is part of the binary pattern is clearly visible.

watermark visibility as an image artifact under daylight illumination, we performed both subjective and objective evaluations.

For both evaluations we used the same test images—we selected five test images from publicly available image datasets, like CID:IQ,[23] CSIQ[24] and Kodak,[25] to include a wide range of lightness and hues. The size of all test images is $800 \times 800$ pixels. They are shown in Figure 5. The embedded binary watermark pattern for all of the test images is shown in Fig. 3 (right). Figure 6 shows the test images watermarked using $\alpha = 3$, as captured by Nikon D610 camera under D50 illumination (top row), and under indoor office illumination plus UV light (bottom row). The UV light source used is the Inova X5 UV flashlight; the distance between the UV flashlight and the printed images was about 10 cm—enough to illuminate the whole image.

***Subjective Evaluation***

We did a simple subjective experiment to evaluate the perceptibility of the hidden pattern under normal light (D50 daylight), and the visibility of the hidden pattern under UV light. We used three different values for the watermark strength $\alpha(\alpha \in \{2, 3, 4\})$ for each of the five test images. The constant $k$ was set to $k = 10^{-3}$. Together with their non-watermarked versions, the total number of printed images used was 20. For the referent D50 and UV diffused light sources, we used the Just Normlicht Color Communicator 2 and X-Rite SpectraLight III viewing booths, respectively. The UV illumination from the X-Rite SpectraLight III viewing booth is significantly weaker than the one from Inova X5 UV flashlight, which results in lower visibility of the watermark. However, for our subjective evaluation we decided to use the viewing booth in order to attain consistency of the UV illumination. The ambient office light was dimmed during both D50 and UV sessions. Eighteen subjects with normal or corrected-to-normal color vision participated in the subjective evaluation. The images were shown to the subjects in a pre-randomized order from a viewing distance of approximately 50 cm, at a viewing angle of around 90°. We observed that the watermark visibility

Figure 5. Test images used for the evaluation, from left to right indexed as 1–5.

Figure 6. Watermarked test images using $\alpha = 3$, as seen under D50 illumination (top row) and indoor office light plus UV flashlight from approximately 10 cm distance (bottom row).

**Table II.** Average percentage of "Yes" answers for the two runs, using D50 light source.

| Image index: | $\alpha = 0$ (no WM) | $\alpha = 2$ | $\alpha = 3$ | $\alpha = 4$ |
|---|---|---|---|---|
| 1 | 5.6 | 5.6 | 11.1 | 25 |
| 2 | 0 | 2.8 | 0 | 2.8 |
| 3 | 0 | 0 | 30.6 | 61.1 |
| 4 | 0 | 63.9 | 69.5 | 86.1 |
| 5 | 0 | 5.6 | 41.7 | 66.7 |
| Average | 1.1 | 15.6 | 30.6 | 48.3 |

is nearly independent of the viewing angle; even angles as low as 20° are suitable for easy watermark detection under the diffused UV illuminant. There were no visible specular reflections from the prints. Each of the subjects viewed the 20 images in two separate runs, for the two different light sources. The order of these four runs was: D50-UV-D50-UV, and there was no break between the four sessions. The subjects were asked to answer with "Yes" or "No" to the following question: "Is there a watermark in the image?" Before the runs, subjects were shown the pattern (Fig. 3 right) which "may have been hidden in some of the images." Table II presents the average percentage of "Yes" answers of all subjects and for the two runs, using the D50 light source. As expected, the perceptibility of the hidden watermark pattern under daylight becomes higher as $\alpha$ increase. The perceptibility in the second D50 run on average was slightly higher than in the first D50 run, as the subjects had already seen what the hidden pattern looks like when embedded in the test images. The intra-subject average percentage of identical answers between the two runs were 84.4% and 96.7% for the D50 and UV sessions respectively. The average percentage of identical answers between subjects (inter-subject, everyone compared against the rest) were 80.2% and 96.3% for the D50 and UV sessions, respectively. Under D50 illumination, the pattern was easier to detect in smoother and homogeneous areas, while in highly textured and noisy areas, like in the 2nd image, the subjects could not detect the pattern even for high values of $\alpha$. The high perceptibility of the pattern for the 4th image even for the lowest $\alpha$ is due to the blue sky area. Apart from the smoothness of the sky area, the bluish colors in general gave higher visibility of the hidden pattern under D50. One of the reasons for this is the low weighting factor for the $b$ channel ($w_b = 0.15$), which reduces the contribution of the error in the $b$ channel to the overall error during the iterative minimization. While the same occurs for the yellowish colors on the other side of the $b$ axis, it turned out that it is not critical due to the lower sensitivity of

**Table III.** Average percentage of "Yes" answers for the two runs, using UV light source.

| Image index: | $\alpha = 0$ (no WM) | $\alpha = 2$ | $\alpha = 3$ | $\alpha = 4$ |
|---|---|---|---|---|
| 1 | 0 | 97.2 | 97.2 | 100 |
| 2 | 0 | 88.9 | 88.9 | 100 |
| 3 | 0 | 97.2 | 100 | 100 |
| 4 | 0 | 97.2 | 100 | 100 |
| 5 | 0 | 100 | 100 | 100 |
| Average | 0 | 96.1 | 97.2 | 100 |

the human visual system in brighter yellow areas than in darker blue areas. Two subjects answered "Yes" when there was no watermark embedded ($\alpha = 0$)—hence the 5.6% for the first image in Table II. Both of these incorrect answers occurred in the first D50 run, when subjects still have not got clear impression of the location/appearance of the embedded watermark; the unfamiliarity with the image, and the mottled type of texture in the background of the first image, might have inclined these two subjects into thinking that the image is watermarked.

Table III presents the average percentage of "Yes" answers averaged from all subjects and for the two runs under UV illumination. The perceptibility of the pattern was very high even for the lowest value of $\alpha$. Only the second image might have been challenging for few of the subjects, as the noisy and textured areas through the whole image mask the hidden watermark. The average time needed for answer per single image viewed under D50 was around 6 seconds, while for the UV runs it was just above 1 second. This considerable difference can be used as an indicator of the difficulty in judging whether the image is watermarked, when viewed under the two different illuminants.

### *Objective Evaluation*

We also performed an objective evaluation of the introduced distortion due to the white modulation. We used the S-CIELAB metric[26] to compare scanned watermarked images with non-watermarked ones, in a framework similar to that of Pedersen and Amirshahi.[27] We used the Epson 10000XL scanner with all color management options switched off. Using the same 1072 patches from the $2 \times 2$ dot-centering printer model, we calibrated a transform from scanner RGB to XYZ (absolute colorimetric with D50 white point) using the Color Engineering Toolbox;[28] it uses 3rd order polynomials for least squares fitting between the two 3D spaces. The average $\Delta E_{94}$ error when fitting the 1072 calibration patches was 0.012. All of the 20 images used in the subjective evaluation were scanned at 600 dpi, resized, aligned and cropped back to $800 \times 800$ pixels. We run the S-CIELAB metric on the whole images, and separately on the areas that correspond to the white and black pixels of the watermark pattern. The viewing distance parameter was set to 50 cm. The results are shown in Table IV. As expected, the $\Delta E_{94}$ distance increases as $\alpha$ increase. The obtained $\Delta E_{94}$ values are relatively low, even for the 4th test image where the hidden pattern was easily perceptible in the sky area. It can also be seen that the S-CIELAB $\Delta E_{94}$ shifts introduced due to enforcing (maximizing) and reducing (minimizing) white pixels are relatively similar for a given $\alpha$, with the areas with minimized white pixels having on average slightly higher $\Delta E_{94}$ value. Overall, the S-CIELAB values are close to the range of what can be considered as just noticeable,[26] and the results of this objective evaluation are fairly consistent with the results obtained in the subjective evaluation.

## CONCLUSION

In this work, we proposed a modification of the CDBS halftoning algorithm, which provides means for hiding visual data in printed color images. The hidden data is detected visually by using a UV light source. The carrier of the hidden signal is the paper fluorescence, which is modulated with the fractional coverage of white-paper area. We used the CIELAB space for the iterative error minimization in the joint CDBS-like halftoning and watermarking approach. The $2 \times 2$ dot-centering model was used for the CMY printer characterization. It is important to note that the strength of the UV watermark depends both on the paper substrate and the UV illuminant used for detection. Papers with higher amount of OBAs are preferred, as well as stronger UV light sources. In our evaluation, we used coated paper,

**Table IV.** S-CIELAB $\Delta E_{94}$ metric between non-watermarked and watermarked scanned images.

| Image index | Average $\Delta E_{94}$ for whole image area | | | Average $\Delta E_{94}$ for image area with maximized number of white pixels | | | Average $\Delta E_{94}$ for image area with minimized number of white pixels | | |
|---|---|---|---|---|---|---|---|---|---|
| | $\alpha = 2$ | $\alpha = 3$ | $\alpha = 4$ | $\alpha = 2$ | $\alpha = 3$ | $\alpha = 4$ | $\alpha = 2$ | $\alpha = 3$ | $\alpha = 4$ |
| 1 | 1.53 | 1.61 | 2.00 | 1.47 | 1.61 | 1.82 | 1.55 | 1.61 | 2.07 |
| 2 | 1.83 | 1.97 | 2.52 | 1.75 | 1.88 | 2.27 | 1.86 | 2.01 | 2.61 |
| 3 | 1.47 | 1.66 | 2.12 | 1.40 | 1.54 | 1.72 | 1.50 | 1.71 | 2.27 |
| 4 | 1.66 | 1.96 | 2.15 | 1.67 | 2.02 | 2.06 | 1.66 | 1.94 | 2.17 |
| 5 | 1.50 | 1.54 | 1.78 | 1.31 | 1.26 | 1.35 | 1.57 | 1.64 | 1.94 |
| Average | 1.60 | 1.75 | 2.11 | 1.52 | 1.66 | 1.84 | 1.63 | 1.78 | 2.21 |

an off-the-shelf UV flashlight, and a UV lamp (in the viewing booth) that was weaker than the UV flashlight. The results from both subjective and objective evaluation showed that this method achieves low perceptibility of the embedded watermark under normal illumination, while attaining watermark UV-signal strength that is reasonably high for many practical applications. This method can be used for robust visual data hiding in natural images with arbitrary content—though the most suitable type of image content is low-to-moderately textured areas, with mid-range values for the lightness.

The next steps to improve the performance of the proposed method, by even further reducing the watermark perceptibility under normal light and/or increasing its visibility under UV light, may include: more detailed investigation and optimization of the CDBS-WM parameters; investigation of other printer models which may use separate characterizations with/without UV included; investigation of using multi-channel printers, as more inks may offer greater flexibility in modulating the white coverage (or the UV-blocking inks coverage); investigation of the use of masking models for content-dependent watermark strength—apart from the aspect of image quality under normal light, masking models can also be used from the aspect of watermark visibility under UV light.

## REFERENCES


[1] I. Cox, M. Miller, and J. Bloom, *Digital Watermarking* (Morgan Kaufmann, San Mateo, CA, 2002).

[2] G. Sharma, *Digital Color Imaging Handbook* (CRC, Boca Raton, FL, 2003).

[3] M. Fu and O. Au, "Watermarking technique for color halftone images," *Proc. Int'l. Conf. on Acoustics, Speech and Signal Processing* (IEEE, Piscatway, NJ, 2004), pp. 381–384.

[4] Y. Guo, O. Au, K. Tang, J. Pang, W. Sun, L. Xu, J. Li, and X. Zhang, "Data Hiding in Error Diffused Color Halftone Images," *Proc. Int'l. Symposium on Circuits and Systems* (IEEE, Piscataway, NJ, 2013), pp. 2996–2999.

[5] B. Oztan and G. Sharma, "Clustered-dot color halftone watermarks using spatial frequency and color separability," Proc. SPIE **7528**, 75280Y (2010).

[6] B. Oztan and G. Sharma, "Per-separation clustered-dot color halftone watermarks: separation estimation based on spatial frequency content," J. Electron. Imaging **19**, 043007 (2010).

[7] B. Oztan and G. Sharma, "Continuous phase-modulated halftones," IEEE Trans. on Image Processing **18**, 2718–2734 (2009).

[8] G. Sharma and S. Wang, "High contrast stochastic screen watermarks for color halftone prints," *Proc. Int'l. Conf. on Image Processing* (IEEE, Piscatway, NJ, 2012), pp. 833–836.

[9] R. Bala, K. M. Braun, and R. P. Loce, "Watermark encoding and detection using narrowband illumination," *Proc. IS&T/SID CIC17: 17th Color Imaging Conf.* (IS&T, Springfield, VA, 2009), pp. 139–142.

[10] R. Eschbach, R. Bala, M. Maltz, and I. Zhao, "Creating variable data signals for security applications," Proc. SPIE **6807**, 68070K (2008).

[11] R. Bala, R. Eschbach, and Y. Zhao, "Substrate fluoroscence: bane or boon?," *Proc. IS&T/SID CIC15: 15th Color Imaging Conf.* (IS&T, Springfield, VA, 2007), pp. 12–17.

[12] Y. Zhao and S. Wang, "UV fluorescence encoded image using two halftoning strategies," Proc. SPIE **7866**, 78661D (2001).

[13] A. U. Agar and J. Allebach, "Model-based color halftoning using direct binary search," IEEE Trans. Image Process. **14**, 1945–1959 (2005).

[14] S. Wang, K. Knox, and N. George, "Novel centering method for overlapping correction in halftoning," *Proc. IS&T 47th Annual Conf. ICPS: The Physics and Chemstry of Imaging Systems* (IS&T, Springfield, VA, 1994), pp. 482–486.

[15] M. Analoui and J. Allebach, "Model-based halftoning using direct binary search," Proc. SPIE **1666**, 96–108 (1992).

[16] D. J. Lieberman and J. Allebach, "A dual interpretation for direct binary search and its implications for tone reproduction and texture quality," IEEE Trans. Image Process. **9**, 1950–1963 (2000).

[17] T. J. Flohr, B. W. Kolpatzik, R. Balasubramanian, D. A. Carrara, C. A. Bouman, and J. P. Allebach, "Model-based color image quantization," Proc. SPIE **1913**, 270–281 (1993).

[18] V. Kitanovski and M. Pedersen, "Orientation modulation for data hiding in chrominance channels of direct binary search halftone prints," J. Imaging Systems and Technology **60**, 50407 (2016).

[19] R. Näsänen, "Visibility of halftone dot textures," IEEE Trans. on Systems, Man, and Cybernetics **SMC-14**, 920–924 (1984).

[20] W. Jiang, W. Xi, U. Sarkar, R. Ulichney, and J. P. Allebach, "Color halftoning based on Neugebauer Primary Area Coverage," *IS&T Electronic Imaging: Color Imaging XXII* (IS&T, Springfield, VA, 2017), pp. 91–102.

[21] D. Lieberman and J. Allebach, "Efficient model based halftoning using direct binary search," *Proc. IEEE Int'l. Conf. on Image Processing* (IEEE, Piscataway, NJ, 1997), pp. 775–778.

[22] X. Zhang and J. P. Allebach, "Quad-interleaved block level parallel direct binary search algorithm," *IS&T Electronic Imaging: Color Imaging XXI* (IS&T, Springfield, VA, 2016), pp. 1–6.

[23] X. Liu, M. Pedersen, and J. Y. Hardeberg, "CID:IQ - a new image quality database," *Proc. Int'l. Conf. on Image and Signal Processing* (Springer, Cherbourg, France, 2014), Vol. 8509, pp. 193–202.

[24] E. C. Larson and D. M. Chandler, "Most apparent distortion: full-reference image quality assessment and the role of strategy," J. Electronic Imaging **19**, 011006 (2010).

[25] Kodak lossless true color image suite, http://r0k.us/graphics/kodak.

[26] X. Zhang and B. A. Wandell, "A spatial extension of CIELAB for digital color image reproduction," *Journal of the Society for Information Display 96 Digest* (John Wiley and Sons, 1996), pp. 731–734.

[27] M. Pedersen and S. A. Amirshahi, "Framework for the evaluation of color prints using image quality metrics," *Proc. IS&T CGIV2010: 5th European Conf. on Colour in Graphics, Imaging, and Vision* (IS&T, Springfield, VA, 2010), pp. 75–82.

[28] P. Green and L. MacDonald, *Colour Engineering: Achieving Device Independent Colour* (Wiley, Chichester, United Kingdom, 2002).